Letter

Doniach phase diagram for the Kondo lattice model on square and triangular lattices

Ruixiang Zhou [1], Xuefeng Zhang,[1] and Gang Li [1,2,*]

[1]School of Physical Science and Technology, ShanghaiTech University, Shanghai 201210, China

[2]ShanghaiTech Laboratory for Topological Physics, ShanghaiTech University, Shanghai 201210, China

(Received 9 February 2023; revised 12 May 2023; accepted 16 May 2023; published 25 July 2023)

In this study we systematically investigate the interplay between Ruderman-Kittel-Kasuya-Yosida (RKKY) and Kondo couplings in the Doniach phase diagram on square and triangular lattices using advanced many-body techniques. Our findings indicate that the simple Doniach phase diagram is inadequate to fully capture the complexity of the competition even on these simple lattices. First, we discovered that the potential energy arising from geometric frustration is comparable to that of RKKY coupling, effectively suppressing long-range antiferromagnetic (AFM) order on the half-filled triangular lattice. Second, while long-range AFM order can be successfully established on the square lattice, Kondo singlets begin to form within the long-range magnetic phase. Upon doping with holes, geometric frustration on the triangular lattice is partially relieved, giving rise to two distinct magnetic orders that emerge unexpectedly. These orders are intimately linked to the topology of the interacting Fermi surface. Our comprehensive analysis of the Kondo lattice model on both lattices reveals a significant interplay between geometric frustration as well as RKKY and Kondo couplings in low-dimensional systems and offers valuable insights into the discovery of novel phases in related materials.

DOI: 10.1103/PhysRevResearch.5.L032014

Introduction. Heavy fermion compounds are strongly correlated electron systems with an extraordinarily large effective electron mass, as experimentally reflected in the large linear T dependence of the specific heat, i.e., $C_V = \gamma T$, as well as the enhanced Pauli susceptibility $\chi(T)$ at temperatures below the so-called Kondo temperature T_K [1–5]. An accepted low-energy description of the heavy fermion systems is the Kondo lattice model (KLM) [6]. In this model, conduction electrons scatter from local moments with coupling strength J. There are two fundamental energy scales in this model. One is the superexchange coupling between local moments mediated by the conduction electrons, which was first considered by Ruderman and Kittel [7] and then further elaborated by Kasuya [8] and Yosida [9], which is now known as the Ruderman-Kittel-Kasuya-Yosida (RKKY) interaction $K \propto J^2$. On the other hand, when J is large, driven by the antiferromagnetic coupling J, some conduction electrons form a spin singlet with the local moment and lose their mobility below T_K. The local moment is screened by the spin of these conduction electrons as if it were effectively removed from the system. This process is known as the Kondo screening. Other electrons will no longer experience the presence of the local moment but only scatter over an effective potential, leading to their Fermi liquid behavior [10,11].

The RKKY interaction and the Kondo screening dominate in the small and large Kondo coupling J region and strongly compete in the intermediate regime, qualitatively described by the Doniach phase diagram [12,13]. In this Letter we want to carefully compare the Doniach phase diagram of the square and triangular lattices with an advanced many-body algorithm, i.e., the dual-fermion (DF) approach [14–17]. It is a nonlocal extension of the dynamical mean-field theory (DMFT) [18–21] and has been verified against numerically exact methods [22]. (See the Supplemental Material for more details [23].) The different lattice geometries add an additional ingredient to the conduction electrons, which itself can mediate their magnetic couplings. The qualitative difference between the RKKY interactions and Kondo screening on the two different lattices is an interesting issue to understand. Although many theoretical studies have been conducted for the KLM and other related models [19–21,24–33], a decent comparison of the two lattices in the same theoretical framework over a wide temperature and doping regime, from which we expect to extract a convincing conclusion on their characteristic difference, is still lacking.

Doniach phase diagram at half filling. The most striking difference of the KLM on the square and triangular lattices is the absence of the long-range magnetic order of the conduction electrons in the RKKY regime on the triangular lattice [see Fig. 1(b)]. On the square lattice, we observe a well-defined antiferromagnetic (AFM) long-range order with magnetic wave vector $\vec{Q} = (\pi, \pi)$ [Fig. 1(a)]. The finite-temperature AFM phase is due to the approximation inherent in our many-body algorithms (see the Supplemental Material [23] for an introduction to the methodology). In real materials, the presence of other types of magnetic interaction, for example, spin anisotropy [34–36], can stabilize the AFM phase at

*ligang@shanghaitech.edu.cn

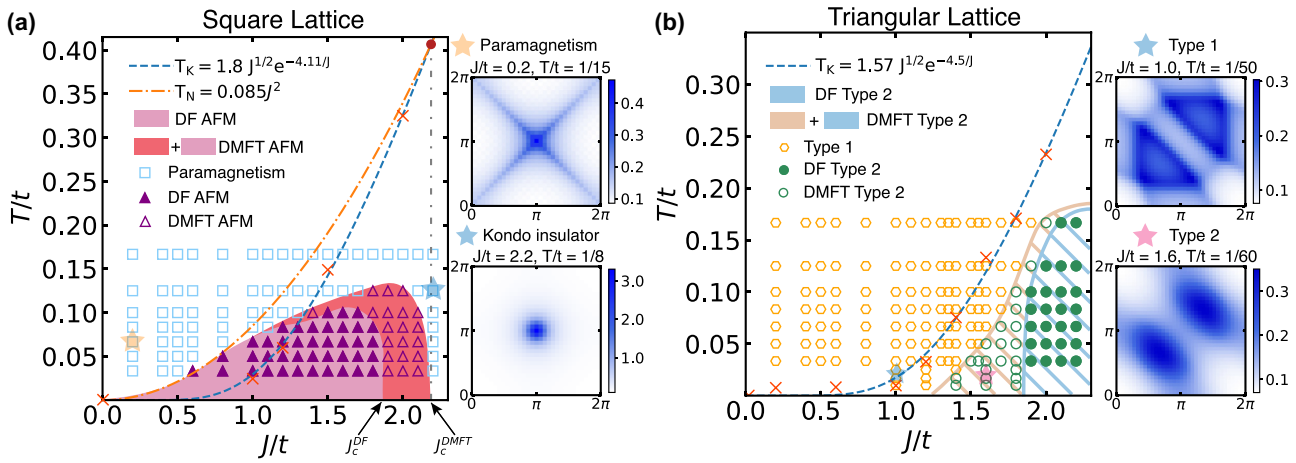

FIG. 1. Doniach phase diagram for the half-filled square and triangular lattices. (a) On the square lattice, the RKKY coupling induces a long-range AFM order in a small to intermediate J regime highlighted in color. The pink and red regions correspond to the AFM phase from the DF and DMFT calculations, respectively. The different symbols denote the different solutions from the two methods. The T_N and T_K were obtained from the AFM phase boundary and the inverse DMFT uniform susceptibility. On the right-hand side, the two spin susceptibility plots correspond to two characteristic parameters for the paramagnetic metal and Kondo insulator with $J/t = 0.2/2.2$ and $T = 0.05/0.10$, respectively. (b) On the triangular lattice, long-range AFM order is absent. The Kondo coupling is the only dominant energy scale. Two characteristic spin susceptibility behaviors were observed and are denoted by type 1 and type 2, corresponding to the yellow and green circles, respectively. Examples of the two susceptibilities are shown on the right plots with $J/t = 1.2/1.6$ and $T/t = 0.1667$. The hatched region corresponds to the parameters where spin susceptibility displays a typical 120° AFM correlation (type 2), but no long-range order.

finite temperature and be compatible with the Mermin-Wigner theorem [37]. The access of the local uniform susceptibility and its fluctuations calculated in DMFT allows us to extract the Kondo temperature $T_K \sim 1.8J^{1/2}e^{-4.11/J}$ for the square lattice and $T_K \sim 1.57J^{1/2}e^{-4.5/J}$ for the triangular lattice shown as the blue dashed line in Fig. 1 [12,38]. The crossing point of T_K and T_N nicely coincides with J_c^{DMFT} estimated from the destruction of the AFM phase in DMFT on the square lattice.

The obvious difference in the KLM on square and triangular lattices highlights the underlying geometrical influence on the conduction electrons. In addition to the competition between the RKKY and Kondo couplings, the geometrical frustration further competes with the two coupling strengths, destroying the long-range AFM order in the weak-J regime on the triangular lattice. Later in the discussion for the hole-doping KLM, we will further see that hole doping partially releases the geometrical frustration and the two lattices again give unexpected differences in magnetic response.

After understanding the Doniach diagram, we further discuss the metal-insulator transition (MIT) phase boundary, which is not shown in Fig. 1 but jointly determines the ground state of the KLM with the Doniach phase diagram. The study of the MIT amounts to calculating the local density of states, which relates to the imaginary part of the single-particle Green's function as $A(\omega) = -\sum_{\vec{k}} \mathrm{Im}G(\vec{k},\omega)/\pi$. At half filling, the KLM on both the square and triangle lattices can develop a charge gap, giving rise to the possibility of forming both a Kondo metal and a Kondo insulator in the KLM.

In Fig. 2 the metallic and insulating solutions are shown by different symbols shaded light red and light cyan. We observe that the MIT phase boundary moves to a smaller J_c with the decrease of temperature on both lattices, displaying a left-going phase boundary. On the square lattice, the MIT phase boundary is under the dome of the AFM phase in Fig. 1(a), separating it into two parts. In the weak-J regime, the conduction electrons are itinerant and AFM ordered corresponding to RKKY metals. For intermediate J, where the RKKY and Kondo couplings strongly compete,

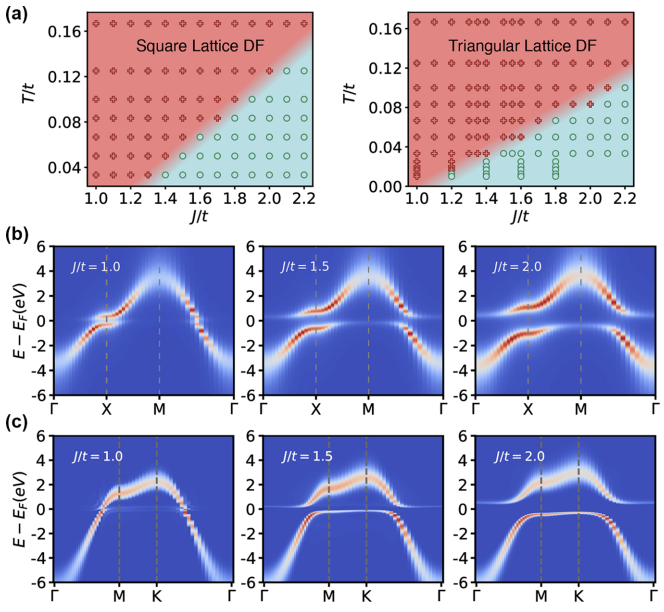

FIG. 2. The MIT phase diagram and spectral functions of the KLM on the square and triangle lattices. (a) The MIT phase boundary for the KLM on the square and triangle lattices. (b) Spectral function along Γ-X-M-Γ at $T/t = 0.04$ and with three different couplings J/t on the square lattice. (c) Same results as in (b) but for the triangular lattice. All results in this figure are obtained with the DF method.

the low-temperature states are insulating, which can be either RKKY-type insulators with long-range AFM order or Kondo insulators with spin singlets depending on the temperature. For large $J > J_c^{\mathrm{DMFT}} \sim 2.2 > J_c^{\mathrm{DF}} \sim 1.8$, these states belong to Kondo insulators on the square lattice. On the triangular lattice, the situation becomes much simpler. As there is no AFM long-range order on the triangular lattice, for any parameter (J, T) the MIT boundary shown in Figs. 2(c) and 2(d) is then the phase boundary for the Kondo metal and Kondo insulator at sufficiently low temperature.

We note that the MIT boundary was obtained with a paramagnetic condition. As magnetic long-range order can gap the conduction electrons, we suspect that in a spin-polarized calculation, the MIT will occur for a smaller critical J/t on the square lattice [39]. However, due to the geometric frustration, no magnetic order is stabilized on the triangular lattice. The nature of the MIT on the triangular lattice is then a paramagnetic phase transition. Kondo coupling becomes the only dominant energy scale on the half-filled triangular KLM.

The presence of the AFM phase on the square lattice has stimulated an interesting issue concerning the existence of the Kondo screening inside the magnetic phase, which is not adequately described by the simple Doniach phase diagram with only one quantum critical point [40–42]. The RKKY-driven long-range magnetic order may not break down at the same J_c where the Kondo singlets start to form. The Kondo singlet already forms inside the long-range antiferromagnetic phase. Only in the weak-coupling regime does the Kondo breakdown occur [43].

Our results on the spectral function shown in Figs. 2(b) and 2(c) support this idea [26,43–45]. On the square lattice, at $J/t = 1.5$ where the AFM order is present, the spectral function shows a clear flat band extending from X and Γ to M, which is already similar to that in the Kondo insulating phase with $J/t = 2.0$. Furthermore, on the triangular lattice, due to the weak competition of the RKKY coupling, the flat bands around the Fermi level are more easily established for the same parameter, confirming the dominant role of the Kondo coupling in the triangular lattice.

The appearance of the flat bands inside the conduction electron spectra clearly shows that the simple Doniach phase diagram is not sufficient in describing the competition between the RKKY and the Kondo couplings even on simple lattices such as the square and triangular lattices studied in this work. On one hand, there is no RKKY long-range order observed on the half-filled triangular lattice. On the other hand, on the square lattice, it is clear that the Kondo singlets appear before the long-range antiferromagnetic order breaks down. The induced flat bands in the conduction electron spectra also lead to the appearance of the van Hove singularity (vHS) inside the local density of states (DOS). According to the study and classification in Refs. [46,47], vHS can be of different characters. After fitting the corresponding DOS of Figs. 2(b) and 2(c) for $J/t = 1.5$ and 2.0, we found that vHS induced by the flat bands below the Fermi level is better understood as a high-order vHS with a power-law divergence. However, due to the uncertainty introduced by the maximal entropy method for analytical continuation [48,49], the character of the emerging vHS induced by the Kondo coupling cannot be determined precisely and deserves more study in the future.

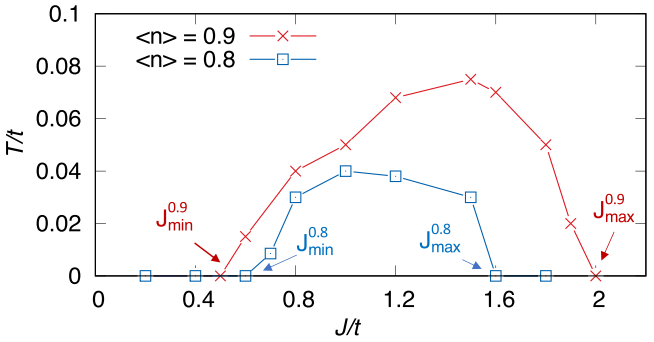

FIG. 3. Magnetic phase diagram of the hole-doped KLM on the square lattice. The magnetic phase boundary is shown for two hole-doping levels. The phase boundary is obtained from a Curie-Weiss fit of the spin susceptibility of the conduction electrons. All results in this figure are obtained with the DF calculations.

Hole doping. After understanding the half-filled case, we now move on to the hole-doped KLM to further understand the persistence of the AFM phase and the emergence of other types of order. One of these phases is the unexpected magnetic long-range order on the triangular lattice. In the following, we will separately discuss the doped KLM on the square and triangular lattices in Figs. 3 and 4, respectively.

Figure 3 displays the magnetic phase diagram of the KLM on the square lattice at two different hole doping levels. For the doped one-band model, there are no correlation-driven or

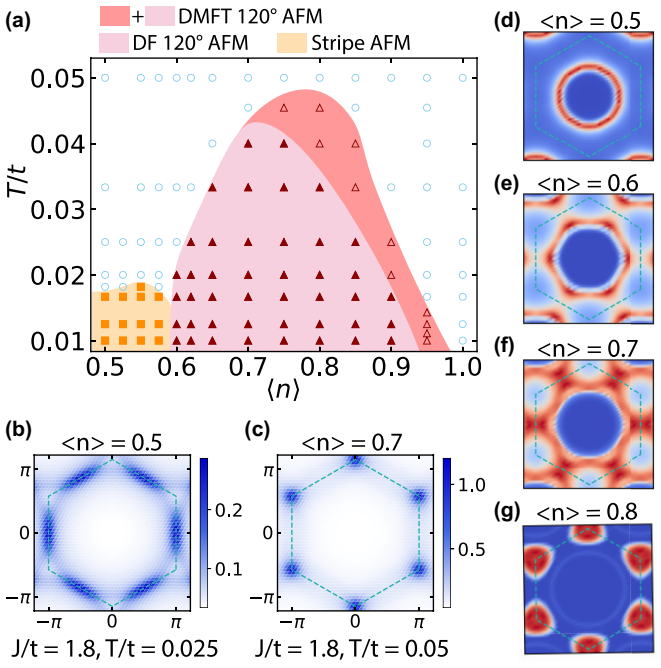

FIG. 4. Magnetic phase diagram of the hole-doped KLM on the triangular lattice. (a) There are two different magnetic orders discovered at different hole doping levels with $J/t = 1.8$. One is the 120° AFM order at $0.6 < \langle n \rangle < 0.9$ and the other is row-wise AFM order at $0.5 < \langle n \rangle < 0.6$. The spin susceptibility is illustrated at (b) $\langle n \rangle = 0.5$ and (c) $\langle n \rangle = 0.7$, displaying different magnetic wave vectors. (d)–(g) Interacting Fermi surface at different electron concentrations.

filling-driven insulating states. States for all of the parameters shown in Fig. 3 are metallic. We observed two characteristic features of the doped KLM on the square lattice. The first one is the shrink of the AFM phase space with the increase of hole doping. With the increase of the hole-doping level, the Néel temperature decreases. Our result is consistent with the observation in the dynamical cluster approximation calculation [26]. Moreover, in the weak-J regime, the AFM phase is completely suppressed. Our finite-temperature calculation does not capture any signature of long-range RKKY order for $J/t < 0.5$. We note that $J_{\max}$, where the AFM order vanishes, becomes slightly larger for $\langle n\rangle = 0.9$ as compared to Fig. 1(a). This can be an artificial effect caused by the fact that we only considered the second DF self-energy diagram and did not employ a full charge self-consistency on both the DMFT and DF levels. Employing the ladder DF self-energy scheme [16] and the full charge self-consistency with the simultaneous convergence of the DMFT and DF solutions will likely reduce $J_{\max}$ to a value smaller than that for half filling, as observed in the single-band Hubbard model [50].

After demonstrating the destruction of the RKKY interactions in the hole-doped KLM on the square lattice, we now turn the focus to the hole-doped triangular lattice. Due to the absence of long-range orders in the half-filled case, we do not expect a considerable difference with hole doping. Similar to the square lattice, we anticipated that hole doping would further suppress the RKKY coupling such that the magnetic phase diagram of the KLM on the triangular lattice would remain completely featureless. Instead, we found a rich magnetic phase diagram as displayed in Fig. 4(a). We discovered two long-range magnetic orders at different doping levels. With the increase of hole doping, we first observe a 120° AFM phase for a wide range of electron occupancy $0.6 < \langle n\rangle < 0.9$, shown as the pink region in Fig. 4(a). The Néel temperature reaches a maximum at $\langle n\rangle \sim 0.7$. Further increasing the hole doping, a new magnetic correlation with row-wise-type spin arrangement appears when the electron occupancy is below $\langle n\rangle < 0.6$. The smallest electron occupancy studied in our work is $\langle n\rangle = 0.5$, which is in the row-wise AFM phase as well.

We attribute the emergence of magnetic orders in the hole-doped triangular KLM to the partial release of geometric frustration and the Fermi surface nesting effect. In comparison to the square lattice, the Fermi surface is not perfectly nested at half filling. There is no spontaneous spin instability for the noninteracting tight-binding model on the triangular lattice. In the Hubbard or periodic Anderson model, only when the coupling between two electrons is strong enough, the classical 120° AFM phase can establish [51–53]. In the KLM, the effective coupling of conduction electrons stems from the superexchange involving two scattering processes at two neighboring sites and the coupling is proportional to J^2. It is easier for the conduction electrons to magnetically order at larger values of J/t, where, however, the formation of the Kondo singlet will strongly compete. Thus, if it exists, the 120° AFM phase will only appear at intermediate J/t at half filling. However, as shown in Fig. 1(b), the superexchange coupling between conduction electrons alone is not sufficient to establish a long-range order before the formation of the Kondo singlet. With hole doping though, the Fermi surface starts to play a role and triggers the emergence of two different magnetic orders.

Away from half filling, the interacting Fermi surface gradually changes topology. We show in Figs. 4(d)–4(g) the Fermi surface obtained as $A(\vec{k}, \omega = E_f) = -\mathrm{Im}G(\vec{k}, \omega)/\pi$ at different electron concentrations. At $\langle n\rangle = 0.6$ and 0.7, the interacting Fermi surface shows a clear hexagonal shape with the nesting vectors corresponding exactly to the **Γ**-**K** vector. Further increasing electron concentration changes the hexagon at **Γ** to six triangles located at the **K** point. The strong density around the **K** point supports coherent scattering between any two **K** points with the scattering vector the same as the **Γ**-**K** vector. The size of the Fermi surface at each **K** becomes smaller with the further increase of concentration, leading to reduced coherence scattering in this case. As a consequence, we found that the Néel temperature reaches a maximum around $\langle n\rangle = 0.7$ and decreases with the increase of electron concentration. At smaller electron occupancy, for example, $\langle n\rangle = 0.5$, the hexagon Fermi surface shrinks to a circle around **Γ** point. A circular Fermi surface does not have nesting vectors and usually does not trigger any magnetic instability. In fact, at half filling the Fermi surface of the tight-binding model on the triangular lattice is also a circle and, as we know, no magnetic long-range order can be established. Here, at $\langle n\rangle = 0.5$, the diameter of the interacting circular Fermi surface is the same as the **Γ**-**M** vector. Both the intra- and inter-Fermi surface scatterings with this wave vector coherently contribute to the magnetic instability, leading to the peak structure of the spin susceptibility with the same wave vector shown in Fig. 4(b). At half filling, however, the intra- and inter-Fermi surface scatterings correspond to different wave vectors and cannot form coherence.

Discussion and conclusions. The square and triangular lattices differ in their geometry and frustration to the long-range spin arrangement. There have been many theoretical studies of correlated models, such as the Hubbard model [52–65], on these two lattices, which establish a fruitful understanding of the different electronic and magnetic responses on them. However, the KLM has not been thoroughly understood and compared on the two lattices.

Our first important observation is the different magnetic responses of the half-filled KLM on the square and triangular lattices. The presence or absence of long-range AFM order on the square and triangular lattices indicates that the RKKY exchange coupling, as a superexchange coupling involving multiple Coulomb scattering processes, is sensitive and comparable in energy scale to the potential created by geometric frustrations. In comparison to the Hubbard model on the triangular lattice, in which the strong Coulomb repulsion is able to stabilize long-range AFM order, the KLM on the triangular lattice is featureless, with the Kondo coupling being the only dominant energy scale.

However, in doping with holes, more exotic differences appear. The KLM on the square lattice shows the expected destruction of the AFM long-range order with the increase of hole concentration, while on the triangular lattice, two magnetic phases appear unexpectedly at different hole doping levels. A 120° AFM phase emerges for a wide range of electron occupancy $0.6 < \langle n\rangle < 0.9$. Within $0.5 < \langle n\rangle < 0.6$, a row-wise-type AFM phase with the magnetic wave

vector $\vec{Q} = (\pi, 0)$ emerges. The analysis of the interacting Fermi surface leads to our second important observation. We found that the 120° AFM order is induced by the intra-Fermi-surface scattering which shows clear nesting topology and favors the coherent magnetic excitation with wave vector **Γ**-**K**. At higher hole doping, the Fermi surface topology transforms to a circular shape. The coherent scattering of the intra- and inter-Fermi-surface scattering promotes a row-wise AFM order. Due to the critical condition and the less strong coherence scatterings, the row-wise AFM phase demonstrates lower Néel temperatures and smaller phase space.

Our systematic study of the KLM on the square and triangular lattices provides deep insight into the underlying competition of the RKKY coupling and the potential energy created by the geometrical frustration. The Doniach phase diagrams and magnetic and electronic excitations of the KLM for both half-filling and doped cases constitute a comprehensive understanding of the KLM on low-dimensional lattices and may pave the way for the study of related materials.

Acknowledgments. G.L. thanks H. Monien, A. Rubtsov, P. Werner, F. Assaad, W. Hanke, R. Thomale, A. I. Lichenstein, and K. Held. This work was supported by the National Key R&D Program of China (Grant No. 2022YFA1402703), National Natural Science Foundation of China (Grant No. 11874263), Shanghai 2021-Fundamental Research Aera (Grant No. 21JC1404700), Shanghai Technology Innovation Action Plan (Grant No. 20DZ1100605), and Sino-German Mobility program (Grant No. M-0006). X.Z. acknowledges Postdoctoral Special Funds for Theoretical Physics of the National Natural Science Foundation of China (Grant No. 12147124). Some of the calculations were performed at the HPC Platform of ShanghaiTech University Library and Information Services and at the School of Physical Science and Technology.

[1] K. Andres, J. E. Graebner, and H. R. Ott, $4f$-Virtual-Bound-State Formation in $CeAl_3$ at Low Temperatures, Phys. Rev. Lett. **35**, 1779 (1975).

[2] P. Fulde, J. Keller, and G. Zwicknagl, *Theory of Heavy Fermion Systems* (Academic, New York, 1988), pp. 1–150.

[3] Y. Ōnuki and T. Komatsubara, in *Anomalous Rare Earths and Actinides*, edited by J. Boucherle, J. Flouquet, C. Lacroix, and J. Rossat-Mignod (Elsevier, Amsterdam, 1987), pp. 281–288.

[4] F. Steglich, U. Rauchschwalbe, U. Gottwick, H. M. Mayer, G. Sparn, N. Grewe, U. Poppe, and J. J. M. Franse, Heavy fermions in Kondo lattice compounds (invited), J. Appl. Phys. **57**, 3054 (1985).

[5] G. R. Stewart, Heavy-fermion systems, Rev. Mod. Phys. **56**, 755 (1984).

[6] P. Coleman, *Introduction to Many-Body Physics* (Cambridge University Press, Cambridge, 2015).

[7] M. A. Ruderman and C. Kittel, Indirect exchange coupling of nuclear magnetic moments by conduction electrons, Phys. Rev. **96**, 99 (1954).

[8] T. Kasuya, A theory of metallic ferro- and antiferromagnetism on Zener's model, Prog. Theor. Phys. **16**, 45 (1956).

[9] K. Yosida, Magnetic properties of Cu-Mn alloys, Phys. Rev. **106**, 893 (1957).

[10] M. Lavagna and C. Pépin, The Kondo lattice model, Acta Phys. Pol. B **29**, 3753 (1998).

[11] M. Gulacsi, The Kondo lattice model, Philos. Mag. **86**, 1907 (2006).

[12] S. Doniach, The Kondo lattice and weak antiferromagnetism, Physica B+C **91**, 231 (1977).

[13] S. Doniach, in *Valence Instabilities and Related Narrow-Band Phenomena*, edited by R. D. Parks (Springer US, Boston, 1977), pp. 169–176.

[14] A. N. Rubtsov, M. I. Katsnelson, and A. I. Lichtenstein, Dual fermion approach to nonlocal correlations in the Hubbard model, Phys. Rev. B **77**, 033101 (2008).

[15] A. N. Rubtsov, M. I. Katsnelson, A. I. Lichtenstein, and A. Georges, Dual fermion approach to the two-dimensional Hubbard model: Antiferromagnetic fluctuations and Fermi arcs, Phys. Rev. B **79**, 045133 (2009).

[16] H. Hafermann, G. Li, A. N. Rubtsov, M. I. Katsnelson, A. I. Lichtenstein, and H. Monien, Efficient Perturbation Theory for Quantum Lattice Models, Phys. Rev. Lett. **102**, 206401 (2009).

[17] G. Rohringer, H. Hafermann, A. Toschi, A. A. Katanin, A. E. Antipov, M. I. Katsnelson, A. I. Lichtenstein, A. N. Rubtsov, and K. Held, Diagrammatic routes to nonlocal correlations beyond dynamical mean field theory, Rev. Mod. Phys. **90**, 025003 (2018).

[18] A. Georges, G. Kotliar, W. Krauth, and M. J. Rozenberg, Dynamical mean-field theory of strongly correlated fermion systems and the limit of infinite dimensions, Rev. Mod. Phys. **68**, 13 (1996).

[19] S. Burdin, D. R. Grempel, and A. Georges, Heavy-fermion and spin-liquid behavior in a Kondo lattice with magnetic frustration, Phys. Rev. B **66**, 045111 (2002).

[20] J. Otsuki, H. Kusunose, and Y. Kuramoto, Evolution of a Large Fermi Surface in the Kondo Lattice, Phys. Rev. Lett. **102**, 017202 (2009).

[21] R. Peters, S. Hoshino, N. Kawakami, J. Otsuki, and Y. Kuramoto, Charge order in Kondo lattice systems, Phys. Rev. B **87**, 165133 (2013).

[22] T. Schäfer, N. Wentzell, F. Šimkovic, Y.-Y. He, C. Hille, M. Klett, C. J. Eckhardt, B. Arzhang, V. Harkov, F.-M. Le Régent, A. Kirsch, Y. Wang, A. J. Kim, E. Kozik, E. A. Stepanov, A. Kauch, S. Andergassen, P. Hansmann, D. Rohe, Y. M. Vilk *et al.*, Tracking the Footprints of Spin Fluctuations: A MultiMethod, MultiMessenger Study of the Two-Dimensional Hubbard Model, Phys. Rev. X **11**, 011058 (2021).

[23] See Supplemental Material at http://link.aps.org/supplemental/10.1103/PhysRevResearch.5.L032014 for details.

[24] P. Fazekas and E. Müller-Hartmann, Magnetic and nonmagnetic ground states of the Kondo lattice, Z. Phys. B **85**, 285 (1991).

[25] C. Lacroix and M. Cyrot, Phase diagram of the Kondo lattice, Phys. Rev. B **20**, 1969 (1979).

[26] L. C. Martin and F. F. Assaad, Evolution of the Fermi Surface across a Magnetic Order-Disorder Transition in the Two-Dimensional Kondo Lattice Model: A Dynamical Cluster Approach, Phys. Rev. Lett. **101**, 066404 (2008).

[27] L. C. Martin, M. Bercx, and F. F. Assaad, Fermi surface topology of the two-dimensional Kondo lattice model: Dynamical cluster approximation approach, Phys. Rev. B **82**, 245105 (2010).

[28] J. Otsuki, H. Kusunose, and Y. Kuramoto, The Kondo lattice model in infinite dimensions: I. Formalism, J. Phys. Soc. Jpn. **78**, 014702 (2009).

[29] J. Otsuki, H. Kusunose, and Y. Kuramoto, The Kondo lattice model in infinite dimensions: II. Static susceptibilities and phase diagram, J. Phys. Soc. Jpn. **78**, 034719 (2009).

[30] Y. Akagi, M. Udagawa, and Y. Motome, Hidden Multiple-Spin Interactions as an Origin of Spin Scalar Chiral Order in Frustrated Kondo Lattice Models, Phys. Rev. Lett. **108**, 096401 (2012).

[31] M. W. Aulbach, F. F. Assaad, and M. Potthoff, Dynamical mean-field study of partial Kondo screening in the periodic Anderson model on the triangular lattice, Phys. Rev. B **92**, 235131 (2015).

[32] M. Keßler and R. Eder, Magnetic phases of the triangular Kondo lattice, Phys. Rev. B **102**, 235125 (2020).

[33] K. Inui and Y. Motome, Channel-selective non-Fermi liquid behavior in the two-channel Kondo lattice model under a magnetic field, Phys. Rev. B **102**, 155126 (2020).

[34] B. Huang, G. Clark, E. Navarro-Moratalla, D. R. Klein, R. Cheng, K. L. Seyler, D. Zhong, E. Schmidgall, M. A. McGuire, D. H. Cobden, W. Yao, D. Xiao, P. Jarillo-Herrero, and X. Xu, Layer-dependent ferromagnetism in a van der Waals crystal down to the monolayer limit, Nature (London) **546**, 270 (2017).

[35] C. Gong, L. Li, Z. Li, H. Ji, A. Stern, Y. Xia, T. Cao, W. Bao, C. Wang, Y. Wang, Z. Qiu, R. Cava, S. G. Louie, J. Xia, and X. Zhang, Discovery of intrinsic ferromagnetism in two-dimensional van der Waals crystals, Nature (London) **546**, 265 (2017).

[36] J. Zhang, X. Cai, W. Xia, A. Liang, J. Huang, C. Wang, L. Yang, H. Yuan, Y. Chen, S. Zhang, Y. Guo, Z. Liu, and G. Li, Unveiling Electronic Correlation and the Ferromagnetic Superexchange Mechanism in the van der Waals Crystal $CrSiTe_3$, Phys. Rev. Lett. **123**, 047203 (2019).

[37] N. D. Mermin and H. Wagner, Absence of Ferromagnetism or Antiferromagnetism in One- or Two-Dimensional Isotropic Heisenberg Models, Phys. Rev. Lett. **17**, 1133 (1966).

[38] P. Coleman, $\frac{1}{N}$ expansion for the Kondo lattice, Phys. Rev. B **28**, 5255 (1983).

[39] S. Hoshino, J. Otsuki, and Y. Kuramoto, Itinerant antiferromagnetism in infinite dimensional Kondo lattice, Phys. Rev. B **81**, 113108 (2010).

[40] V. Y. Irkhin and M. I. Katsnelson, Scaling picture of magnetism formation in the anomalous f-electron systems: Interplay of the Kondo effect and spin dynamics, Phys. Rev. B **56**, 8109 (1997).

[41] V. Y. Irkhin and M. I. Katsnelson, Scaling theory of magnetic ordering in the Kondo lattices with anisotropic exchange interactions, Phys. Rev. B **59**, 9348 (1999).

[42] V. Y. Irkhin and M. I. Katsnelson, Non-fermi-liquid behavior in Kondo lattices induced by peculiarities of magnetic ordering and spin dynamics, Phys. Rev. B **61**, 14640 (2000).

[43] M. Raczkowski, B. Danu, and F. F. Assaad, Breakdown of heavy quasiparticles in a honeycomb Kondo lattice: A quantum Monte Carlo study, Phys. Rev. B **106**, L161115 (2022).

[44] H. Watanabe and M. Ogata, Fermi-Surface Reconstruction without Breakdown of Kondo Screening at the Quantum Critical Point, Phys. Rev. Lett. **99**, 136401 (2007).

[45] B. Danu, Z. Liu, F. F. Assaad, and M. Raczkowski, Zooming in on heavy fermions in Kondo lattice models, Phys. Rev. B **104**, 155128 (2021).

[46] A. Chandrasekaran, A. Shtyk, J. J. Betouras, and C. Chamon, Catastrophe theory classification of Fermi surface topological transitions in two dimensions, Phys. Rev. Res. **2**, 013355 (2020).

[47] N. F. Q. Yuan and L. Fu, Classification of critical points in energy bands based on topology, scaling, and symmetry, Phys. Rev. B **101**, 125120 (2020).

[48] R. N. Silver, D. S. Sivia, and J. E. Gubernatis, Maximum-entropy method for analytic continuation of quantum Monte Carlo data, Phys. Rev. B **41**, 2380 (1990).

[49] M. Jarrell and J. Gubernatis, Bayesian inference and the analytic continuation of imaginary-time quantum Monte Carlo data, Phys. Rep. **269**, 133 (1996).

[50] J. Otsuki, Competing d-Wave and p-Wave Spin-Singlet Superconductivities in the Two-Dimensional Kondo Lattice, Phys. Rev. Lett. **115**, 036404 (2015).

[51] B. Kyung and A.-M. S. Tremblay, Mott Transition, Antiferromagnetism, and d-Wave Superconductivity in Two-Dimensional Organic Conductors, Phys. Rev. Lett. **97**, 046402 (2006).

[52] G. Li, A. E. Antipov, A. N. Rubtsov, S. Kirchner, and W. Hanke, Competing phases of the Hubbard model on a triangular lattice: Insights from the entropy, Phys. Rev. B **89**, 161118(R) (2014).

[53] X. Gao, C. Hu, J. Sun, X.-Q. Wang, H.-Q. Lin, and G. Li, Reentrant metal-insulator transition and competing magnetic interactions on a triangular lattice with second nearest-neighbor hopping, Phys. Rev. B **103**, 235134 (2021).

[54] S. R. White, D. J. Scalapino, R. L. Sugar, E. Y. Loh, J. E. Gubernatis, and R. T. Scalettar, Numerical study of the two-dimensional Hubbard model, Phys. Rev. B **40**, 506 (1989).

[55] C. Gröber, R. Eder, and W. Hanke, Anomalous low-doping phase of the Hubbard model, Phys. Rev. B **62**, 4336 (2000).

[56] H. Lee, G. Li, and H. Monien, Hubbard model on the triangular lattice using dynamical cluster approximation and dual fermion methods, Phys. Rev. B **78**, 205117 (2008).

[57] C. N. Varney, C.-R. Lee, Z. J. Bai, S. Chiesa, M. Jarrell, and R. T. Scalettar, Quantum Monte Carlo study of the two-dimensional fermion Hubbard model, Phys. Rev. B **80**, 075116 (2009).

[58] N. Bulut, D. J. Scalapino, and S. R. White, One-Electron Spectral Weight of the Doped Two-Dimensional Hubbard Model, Phys. Rev. Lett. **72**, 705 (1994).

[59] M. Laubach, R. Thomale, C. Platt, W. Hanke, and G. Li, Phase diagram of the Hubbard model on the anisotropic triangular lattice, Phys. Rev. B **91**, 245125 (2015).

[60] J. Kokalj and R. H. McKenzie, Enhancement of thermal expansion of organic charge-transfer salts by strong electronic correlations, Phys. Rev. B **91**, 205121 (2015).

[61] G. Rohringer and A. Toschi, Impact of nonlocal correlations over different energy scales: A dynamical vertex approximation study, Phys. Rev. B **94**, 125144 (2016).

[62] T. Shirakawa, T. Tohyama, J. Kokalj, S. Sota, and S. Yunoki,

Ground-state phase diagram of the triangular lattice Hubbard model by the density-matrix renormalization group method, Phys. Rev. B **96**, 205130 (2017).

[63] M. Qin, T. Schäfer, S. Andergassen, P. Corboz, and E. Gull, The Hubbard model: A computational perspective, Annu. Rev. Condens. Matter Phys. **13**, 275 (2022).

[64] P. Sahebsara and D. Sénéchal, Hubbard Model on the Triangular Lattice: Spiral Order and Spin Liquid, Phys. Rev. Lett. **100**, 136402 (2008).

[65] S. Li and E. Gull, Magnetic and charge susceptibilities in the half-filled triangular lattice Hubbard model, Phys. Rev. Res. **2**, 013295 (2020).